Multi wavelength stabilization control of thermooptic system with adaptive reconfiguration

ANDRI MAHENDRA[1,2,*], CHUNLE XIONG[2], XIANG ZHANG[2], BENJAMIN J. EGGLETON[2,3], AND PHILIP H. W. LEONG[1,3]

[1] School of Electrical and Information Engineering, University of Sydney, NSW 2006, Australia
[2] Center for Ultrahigh Bandwidth Devices for Optical Systems (CUDOS), Institute of Photonics and Optical Science (IPOS), School of Physics, University of Sydney, NSW 2006, Australia
[3] The Australian Institute for Nanoscale Science and Technology (AINST), University of Sydney, NSW 2006, Australia
[*] Corresponding author: andri.mahendra@sydney.edu.au

Compiled January 5, 2017

Accurate temperature control is crucial for the reliable operation of photonic integrated circuits in the presence of internal thermal crosstalk or external thermal disturbance. We propose an adaptive multiple-input and multiple-output (MIMO) control scheme to stabilize the operation wavelength of on-chip wavelength demultiplexers that have many applications in photonic-chip-based optical signal processing. Using the MIMO control scheme, the wavelength drift is reduced from 0.5 nm to 0.1 nm when internal and external thermal disturbances occur.

OCIS codes: *(130.0130) Integrated optics; (130.0250) Optoelectronics; (130.6622) Subsystem integration and techniques.*

http://dx.doi.org/10.1364/ao.XX.XXXXXX

1. INTRODUCTION

Photonic integrated circuits (PICs) have been proposed for many applications including sensing [1], communication [2] and quantum computing [3]. PICs are often implemented in Complementary Metal-Oxide Semiconductor (CMOS) compatible technologies and the materials involved have high thermooptic coefficients [4], making their operation very sensitive to temperature changes.

Temperature sensitivity can be utilized advantageously. For example, a quantum time-bin entanglement experiment used temperature-dependent tunable couplers and phase shifters to control the amplitude, phase, and wavelength of certain photon states [3]. Fig. 1 shows the schematic of an on-chip wavelength division multiplexer (WDM) based on Mach Zehnder Interferometers (MZIs). Overall, it is a MZI with two arms slightly unbalanced in length. The slight difference in arm lengths determines the free spectral range (FSR) and the phase shifter can vary the peak wavelengths [Fig. 2]. When both input and output couplers are exactly at the 50:50 splitting ratio, the best extinction ratio is achieved. In reality, it is difficult to make on-chip directional couplers with exactly 50:50 splitting ratio due to fabrication imperfections. The solution is to make an arbitrarily tunable coupler based on a MZI with two arms balanced in length, as shown in the dashed rectangles in Fig. 1. In such a balanced MZI, even if the input and output directional couplers deviate from the 50:50 splitting ratio, we can use the phase shifter to control the ultimate splitting ratio. The phase shifters use thermooptic effects through applying a certain voltage to the resistive heaters. Three resistive heaters, controlled by voltages V1, V2 and V3 are used to adjust the refractive index of the waveguide, which allows a controllable phase shift. When this MZIs-based configuration scales up and is integrated into more complicated circuits with multiple inputs, outputs and several functionalities, care must be taken to avoid changes in the output, i.e. signal drift. Thus accurate and robust control of multiple inputs and multiple outputs (MIMO) are required in practical systems.

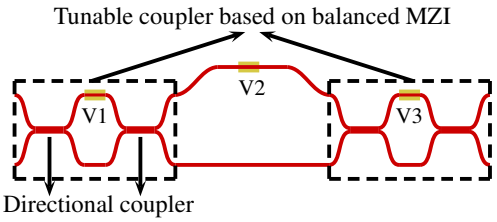

Fig. 1. Schematic of an on-chip MZIs-based WDM. The yellow parts are heaters for thermooptic-based phase shifters. V1, V2, V3 are voltage inputs to adjust refractive index of the waveguide, which enables a controllable phase shift.

Control schemes on photonic based electrooptic and ther-

mooptic system have been proposed for many applications. For instance, ring resonator MIMO based electrooptic systems have been proposed using cascaded microresonator-based matrix switches in a silicon photonic interconnection network for manycore computing applications [5]. The system employed resonator-based electrooptic switches to achieve nonblocking interconnections among multiple inputs and multiple outputs. MZI thermooptic systems with MIMO control is an alternative approach that has versatile functionality and reconfigurability.

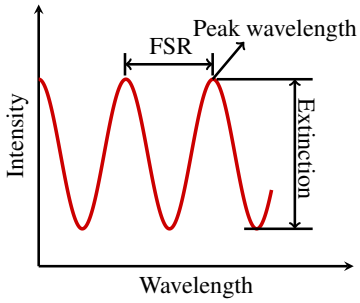

Fig. 2. A typical spectral response of the WDM with a broadband input light source. The red sinusoid line is the light signal which has intensity, wavelength, free spectral range (FSR), peak wavelength and extinction ratio.

Efforts to address the issue of thermal sensitivity are reviewed in reference [6–10], and approaches include athermal waveguides, thermally self-compensating passive circuits and active feedback control. Wavelength locking and thermally stabilized operation were demonstrated using a silicon microring resonator and dithering in a thermally volatile environment [11]. In addition, contactless integrated photonic probe (CLIPP) as input for feedback control for compact system integration was also demonstrated [12]. In 2015, Fisher et al. [13] proposed a control scheme based calibration technique and extremum seeking algorithm on a large PIC incorporating ring resonators and MZI structures; however, there has been no experimental demonstration on MZI-based systems. In addition, the robustness, loop interaction and control are not analyzed and may not yield the best overall control.

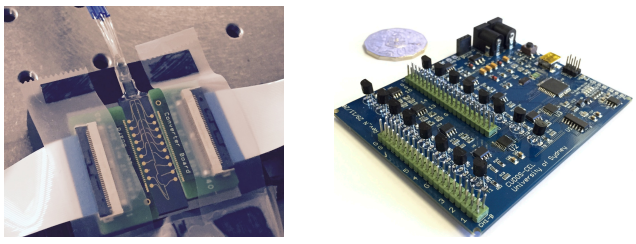

(a) (b)

Fig. 3. (a) a photograph of the Si_3N_4-based MZI thermooptic chip. The yellow parts are wire bonds for heaters, and the green parts are custom printed circuit boards connected via ribbon cable for providing voltage to the heaters. On the top side is the pigtailed fiber array and (b) an integrated 16-channels heater controller with two green connector lines for ribbon cable connection to the heaters on the chip.

In [14], we presented unique design of single input and single output system controller with proportional integral derivative (PID) algorithm for wavelength stabilization with external disturbance. This paper demonstrates, for the first time, MIMO control of a silicon nitride thermooptic PIC incorporating MZIs. This work differs in several aspects including control algorithm, experimental setup, feedback input, circuit under test complexity and disturbance compared with reference [14] . Using a dual proportional integral reference tracking algorithm [15, 16] combined with system identification [17], we demonstrate reliable performance with enhanced reconfigurability. For system identification, the underdamped pair and real pole method is applied for robust analysis [18]. The control system adaptively tunes and maintains the operation wavelength of the target outputs. The system performance was improved in terms of control accuracy by reducing wavelength peak drift due to internal and external disturbances from 0.5 nm to 0.1 nm.

2. EXPERIMENT AND CONTROL SETUP

Our experiment studies a silicon nitride photonic chip. The chip shown in Fig. 3(a) is fabricated using the double-stripe waveguide technology with LioniX BV [19]. The waveguides comprise of SiO_2 cladding and two strips of Si_3N_4 layers stacked on top of each other with SiO_2 as an intermediate layer. The strips are constructed to be 1.5 μm wide, and the Si_3N_4 layers and SiO_2 intermediate layers are formed to be 170 and 500 nm thick, respectively. This allows < 100 μm bending radius with a propagation loss of < 0.2 dB/cm for TE polarization and single mode operation at 1550 nm with a high index contrast. All waveguide inputs and outputs are pigtailed with a polarization maintaining fiber (PMF) array. The layout of the chip is sketched in Fig. 4. Our research focuses on stabilizing the operation wavelengths of the two MZI-based WDMs when internal and external heat disturbances occur, as explained in Fig. 1 and Fig. 2. All heaters that are used to control the phase shift have a nominal resistance of 600 Ω.

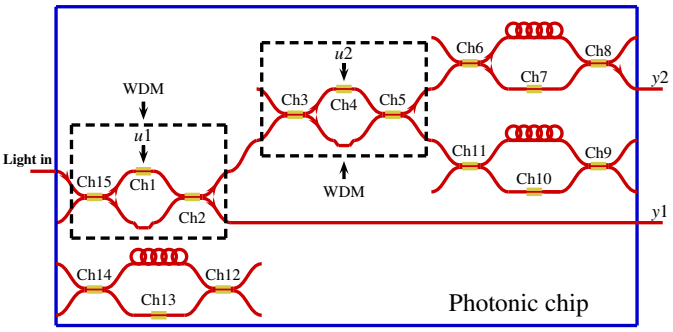

Fig. 4. Chip test setup with two feedback inputs $u1$ and $u2$ and two outputs $y1$ and $y2$; Feedback points are Ch1 and Ch4 (WDM parts); Ch1-Ch15 are heater points inside the chip. The red lines represent the Si_3N_4 waveguides, and the yellow lines are the resistive heaters.

In order to verify our proposed dual proportional integral reference tracking algorithm, the measurement is arranged as shown in Fig. 6. Amplified Spontaneous Emission (ASE) generates a broadband light source in the telecom C-band. The output is controlled with a tunable attenuator, a fiber inline polarizer (IP) and a Polarization Controller (PC). The input power is monitored using a power meter (PM) and a 50:50 fiber coupler. In this experiment, 15 heaters are connected via electrical wires (black lines) bonded directly to the heater controller shown in

Fig. 3(b). The heater controller as shown in Fig. 3(b) consists of 16 channel outputs, 15 of them being used to provide voltages to the heaters on the photonic chip. The hardware is designed specifically based on open source Arduino using ATmega32u4 with two 16-bit Octal Digital Analog Converters (DACs), eight dual amplifiers and 16 voltage follower circuits integrated onto one board. These electronic circuits as shown in Fig. 3(b) could be scaled for more channel outputs. Two outputs of the chips are connected to two Anritsu® MS9740A Optical Spectrum Analyzers (OSA). The OSA is employed to obtain the operation wavelength of the WDMs. These signals are then used as the inputs in our control algorithm.

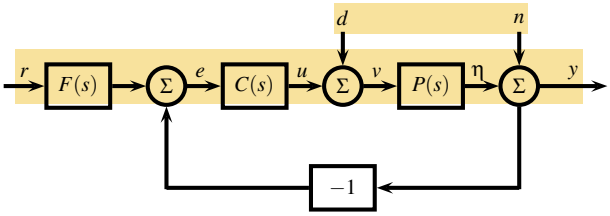

Fig. 5. Basic feedback loop with the assumption that the three components are linear functions of the sums of their inputs. P: plant; C: controller; F: sensor. r: reference or command input; u: actuating signal; d: external disturbance; v: sum (represented by Σ) of actuating signal and disturbance; η: plant output; y: sum of plant output and noise n; n: sensor noise.

In order to provide system summary for analysis and design of the input/output response, the basic control system transfer function for the experiments need to be defined [25]. Consider the system in Fig. 5 has three blocks representing a plant or process P, a feedback controller C and a sensor or feedforward controller F. There are three external signal: the reference r, the measurement noise n and the load disturbance d. A common problem is to find out how the error e is corresponding to the signals r, d and n.

$$e = Fr - y. \tag{1}$$

$$y = n + \eta, \quad \eta = P(d + u), \quad u = Ce. \tag{2}$$

$$\begin{aligned} e = Fr - y = Fr - (n + \eta) = Fr - (n + P(d + u)) \\ = Fr - (n + P(d + Ce)), \end{aligned} \tag{3}$$

To derive the relevant transfer function, it begins with the control error e, given by Eq (1). From the block diagram as shown in Fig. 5, signal y is the sum of n and η, where η is the output of the plant, therefore we can define Eq (2).

$$e = Fr - n - Pd - PCe. \tag{4}$$

$$\begin{aligned} e = \frac{F}{1+PC}r - \frac{1}{1+PC}n - \frac{P}{1+PC}d \\ = G_{er}r + G_{en}n + G_{ed}d, \end{aligned} \tag{5}$$

We obtain Eq (3) by combining Eq (1) and Eq (2). Hence, Eq (4) is the result of this combination. Finally, solving Eq (4) for e produces Eq (5). G is defined as the transfer function.

$$G_{er}r = \frac{F}{1+PC}, \quad G_{en}n = \frac{-1}{1+PC}, \quad G_{ed}d = \frac{-P}{1+PC} \tag{6}$$

The error e is the sum of three terms, depending on the load disturbance d, the reference r and the measurement noise n. The functions in Eq (6) are transfer functions from noise n, reference r and disturbance d to the error e.

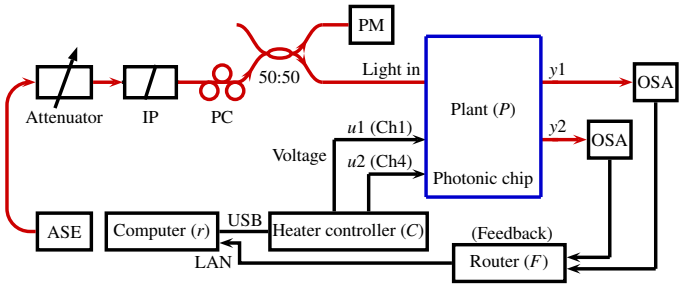

Fig. 6. Experiment setup of MIMO feedback control. Red solid lines are optical fibers, and black solid lines are electric cables. ASE: amplified spontaneous emission; IP: inline polarizer; PC: polarization controller; PM: power meter; OSA: optical spectrum analyzer; LAN: local area network; USB: universal serial bus.

The control feedback system in this paper provides several parameters for the experiment setup shown in Fig. 6. Plant P is represented by the silicon nitride photonic chip and controller C is the heater controller that supplies the voltage to the chip. The objective of the control system is to set the output $y(y1, y2)$ by manipulating input $u(u1, u2)$, the voltage input to the heater. The output y is detected using the OSAs. This output is compared by F to the reference value r. The control objective is to keep $e = y - r$ small. Assume the plant P, controller C and sensor F are linear and time-invariant. The system can be analyzed using the Laplace transform on the variables. This gives the relations as described in Eq (7) and Eq (8). These equations give the $y(s)$ as described in Eq (9) by solving $y(s)$ in term of $r(s)$.

$$y(s) = P(s)u(s), \quad u(s) = C(s)e(s) \tag{7}$$

$$e(s) = r(s) - F(s)y(s) \tag{8}$$

In order to have reference point at a specific wavelength, calibration on applied voltage inputs and correlated wavelength output are conducted. Open loop calibration experiments are carried out by collecting data of applied voltage and wavelength output response. A high speed Agilent® 86115B 10 Gb/s oscilloscope is used to confirm the wavelength outputs. These applied voltages and wavelength outputs data are then used as look up table on programing the feedback control. The feedback control points are at channel 1 and channel 4 on heater controller. The range of the output of OSA 1 or trace window is set to 1558 nm to 1565 nm to avoid double peak detection. The second output at OSA 2 is also fixed to 1543 to 1549 nm for the same reason.

$$y(s) = \frac{P(s)C(s)}{1 + F(s)P(s)C(s)}r(s) \tag{9}$$

3. CONTROL MODEL AND TRANSFER FUNCTION

Feedback control aims to manipulate an output subject to an unknown disturbance, with the goal of minimizing an error function. Multiple input multiple output (MIMO) systems utilize different error functions to single input single output (SISO) and can present a sensitivity to uncertainty which is fundamentally different [21]. MIMO transfer functions utilise vector values for inputs and outputs, and can be specified by concatenation of SISO transfer function models. Eq (10) is based on underdamped pair and real pole which described on reference [18].

$$H(s) = \frac{K}{(T_1 s + 1)(T\omega^2 s^2 + 2\zeta T\omega s + 1)} \quad \textbf{(10)}$$

The transfer function is deduced from the experimental setup via system identification [17]. Once inputs and outputs are obtained from the experimental data, the transfer function is analyzed and the coefficients needed for real control algorithm obtained. The MIMO model generated by this transfer function is described in detail in reference [22]. The transfer function model of the plant for proportional integral reference tracking in this experiment is generated using plant identification system in Matlab® [24], assuming a transfer function H(s) with underdamped pair and real pole as shown in Fig. 7 which is described by Eq (10).

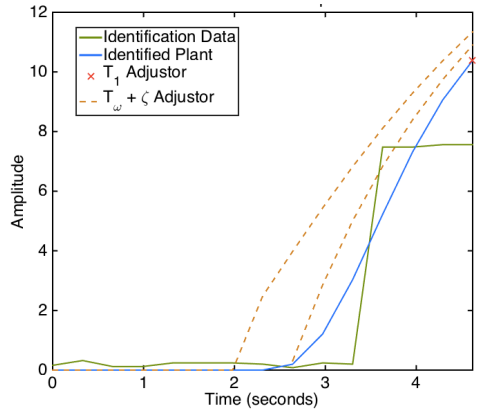

Fig. 7. Control model using underdamped pair and real pole analysis. The green solid line depicts the identified signal from the experiment. The blue solid line shows the identified generated plant model with underdamped pair and real pole analysis. Red cross mark is the the first time constant (T_1) parameter. The dashed orange lines are the natural frequency ($T\omega$) and (the damping coefficient (ζ) parameters used to tune the model.

The configurable parameters include the damping coefficient ζ and the gain K. The other parameters are the first time constant T_1 and the time constant associated with the natural frequency $T\omega$. The estimated parameters for identified plant structure are K = 38.151, T_1 = 2.62, $T\omega$ = 0.41912 and ζ = 0.447. Using proportional integral control with standard tuner and balance settings, the rise time and settling time are 1.21 seconds and 6.72 seconds respectively. The overshoot is about 9.94 %, peak 1.1 and phase margin 60 deg@0.817 rad/s, ensuring closed loop stability.

4. CONTROL SYSTEM TEST

Experiments are carried out to test the performance of the MIMO feedback control system. Three different conditions are used to evaluate the performance. The first test is single closed loop test (SISO) with internal disturbance. The second test is MIMO closed loop with internal disturbance. Finally, the MIMO system test with external disturbance is conducted.

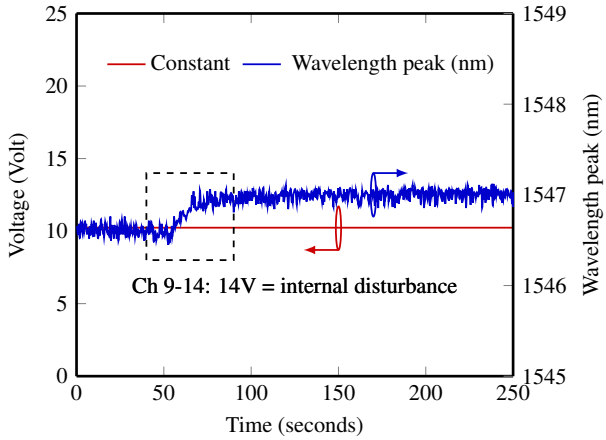

Fig. 8. Internal disturbance quantification from channel 9 to 14. The red line illustrates the voltage constant setting at Ch1. The blue line represents wavelength peak measurements when the voltage applied to the heaters. The wavelength drift starts at around 55 seconds when Ch9-14 are applied with 14 V inputs (internal disturbance).

The closed loop systems are prepared with several procedures. The identification step response was collected from input and output experiments data as described in transfer function model before the control parameters applied into real system. This data then analysed and tuned using system identification system in MATLAB® [17]. The tuned parameters of the proportional integral term were then applied to the system. In order to make feedback control test 1, wavelength output and voltage input were calibrated to acquire a set of targets. By applying voltages at channel 1 from 0 Volt to 14 Volt, the peak wavelength output was varied from 1548.2 nm to 1543.2 nm. For feedback control test 2 at channel 4, changing the heater voltage from 0 to 14 Volt. Resulted in wavelength peak from 1561.2 nm to 1552.88 nm. As the proportional and integral terms depend on coefficient Kp and Ti [25], the optimal values for the proportional and integral terms where 100 and 0.010 for Kp and Ti value.

Several channels are used to create internal disturbance of the photonic chip. Channel 9, 10, 11, 12, 13 and 14 are used to create internal disturbance source by supply 14 Volt for each channel. By activating these channels, the temperature increases because of the heat accumulation created by the channel heaters. This accumulation causes the wavelength drift. The internal disturbance quantification result is shown in Fig. 8. From this figure, the wavelength peak drifts from 1546.5 nm to 1547 nm or about 0.5 nm when the internal disturbance is active. The total of applied power for internal disturbance in this silicon nitride is calculated by $((Vin^2)/Resistance) * Channel\ active)$. The drifts per 1 nm is occurred when the total applied power at 0.32 W.

External disturbance is created by using a hot air blower to heat the silicon nitride chip from about 80 cm for about 15 seconds. The external heat from the blower also creates wavelength

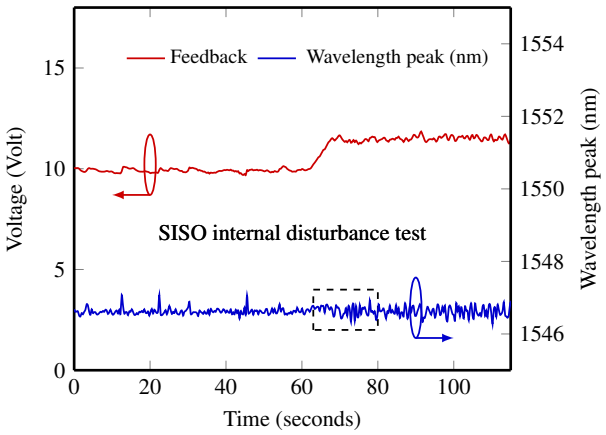

Fig. 9. Single closed loop with internal disturbance test. The red solid line represents feedback voltage input of feedback point at Ch1 of the heater ($u1$). The blue solid line illustrates controlled wavelength peak signal ($y1$). The controller responses the change of wavelength peak when internal disturbance occur at around 65 seconds by adjusting the feedback voltage input.

drift similar to internal disturbance. From the experiments, the temperature sensor shows increasing of temperature to about 34^oC from 24^oC. This setup is used to simulate extreme environment condition or volatile external environment.

Single closed loop test result is shown in Fig. 9. Without internal disturbance, the peak wavelength output is around 1546.6 nm at 10.2 Volt. For this test, internal disturbance is started at about 65 seconds. Fig. 9 shows feedback control system responded the output change and stabilize the output. The response speed of the system was about 0.3 ms which come from sample rate from the OSA through the local area network (LAN) connection.

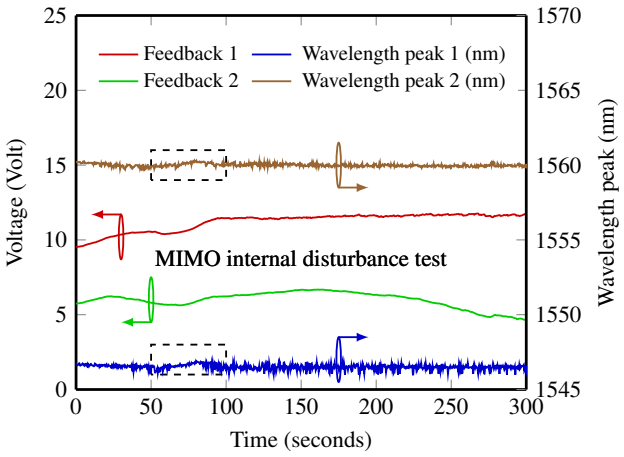

Fig. 10. MIMO closed loop with internal disturbance test. The red line represents feedback voltage input of feedback point at Ch1 of the heater ($u1$). The brown line illustrates controlled wavelength peak signal ($y1$). The green solid line presents as feedback voltage input at feedback point at Ch4 of the heater ($u2$). The blue solid line depicts controlled wavelength peak signal ($y2$). The internal disturbance applies at around 50 seconds.

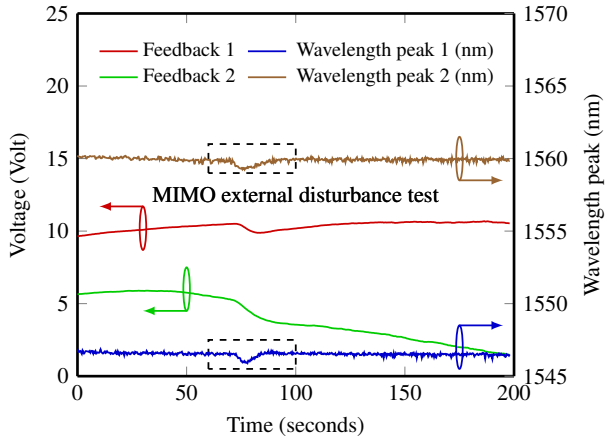

Fig. 11. MIMO closed loop with external disturbance test. The red line represents feedback voltage input of feedback point at Ch1 of the heater ($u1$). The brown line illustrates controlled wavelength peak signal ($y1$). The green solid line presents as feedback voltage input at feedback point at Ch4 of the heater ($u2$). The blue solid line depicts controlled wavelength peak signal ($y2$). The external disturbance applies at around 70 seconds.

For the MIMO test with internal disturbance, the feedback control system is set at channel 1 and channel 4. Channel 2, 3, 5, 6, 7, 8 and 15 voltage inputs are situated as the calibration. Fig. 10 shows the test result with two inputs and two outputs. The two feedback control points at channel 1 and 4 applied tuned robust dual proportional integral reference tracking technique with optimal parameters as described in previous section. The internal disturbance started at around 70 seconds. Two target outputs are fixed at 1546.6 nm at output 1 and 1560.1 nm at output 2. This setup is based on look up table from calibration result of each point to applied voltage correlation. Fig. 10 depicts the two stabilization of two targets, the feedback system adjust the inputs automatically depends on the drift. The two inputs change correspondingly and interact each other to balance the two outputs.

Fig. 11 depicts full system test with external disturbance. The heating started at 70 seconds. During this time, the MIMO closed loop systems also response or compensate the disturbance by adjusting the voltages of both feedback control inputs to the target wavelength peak. In contrast with internal disturbance drift, this disturbance changes the wavelength peak to shift from higher to lower wavelength peak value. This condition is possibly due to random heat effect during hot air blower heating to one of the phase shifter. As shown in Fig. 11, the feedbacks response the drift by lowering the voltage to adjust the wavelength direction to the target.

The present demonstration shows the utility of the approach for dual outputs. The same technique can be extended to larger numbers of inputs and outputs, and is an alternative to other approaches such as dithering [2] and extremum seeking [13], and allows solid control theory to be applied to the problem, leading to a more robust solution with improved transient response. Future work will involve larger degrees of integration, employing schemes such as those of reference [12].

5. CONCLUSION

In conclusion, we proposed a MIMO control with multi proportional integral reference tracking technique combined with system identification scheme to maintain peak wavelength of PICs outputs. The control scheme can then be adaptively tuned by the integrated electronics circuit controller.

We envision that such an adaptively tuned complex Mach Zehnder interferometer structure should constitute a practical building block for reconfigurable and robust photonic systems, with the key advantages of enabling reliable and adaptive reconfiguration of complex photonic integrated circuits.

Funding. Australian Research Council (ARC) Centre of Excellence (CUDOS, CE110001018), Laureate Fellowship (FL120100029), the Discovery Early Career Researcher Award programs (DE120100226) and Indonesia Endowment Fund for Education (LPDP).

Acknowledgment. The authors would like to acknowledge David Marpaung, Calla Klafas, Bryn Bell, Iman Jizan and Jiakun He for discussion.

REFERENCES

1. Q. Liu, X. Tu, K. W. Kim, J. S. Kee, Y. Shin, K. Han, Y. J. Yoon, G. Q. Lo and M. K. Park, "Highly sensitive mach-zehnder interferometer biosensor based on silicon nitride slot waveguide," Sensor and Actuators B: Chemical **188**, 681-688 (2013).
2. K. Padmaraju, K. Bergman, "Resolving the thermal challenges for silicon microring resonator devices," Nanophotonics **3**, 269–281 (2014).
3. C. Xiong, X. Zhang, A. Mahendra, J. He, D. Y. Choi, C. Chae, D. Marpaung, A. Leinse, R. Heideman,M. Hoekman et al., "Compact and reconfigurable silicon nitride time-bin entanglement circuit," Optica **2**, 724–727 (2015).
4. M. S. Nawrocka, T. Liu, X. Wang, and R. R. Panepucci, "Tunable silicon microring resonator with wide free spectral range," Applied physics letters **89**, 71110–71110 (2006).
5. A. W. Poon, X. Luo, F. Xu, and H. Chen, "Cascaded microresonator-based matrix switch for silicon on-chip optical interconnection," Proceedings of the IEEE **97**, 1216–1238 (2009).
6. M. Harjanne, M. Kapulainen, T. Aalto, and P. Heimala, "Sub-s switching time in silicon-on-insulator Mach-Zehnder thermooptic switch," IEEE Photonics Technology Letters **16**, 2039–2041 (2004).
7. R. Amatya, C. W. Holzwarth, H. I. Smith, and R. J. Ram, "Precision tunable silicon compatible microring filters," IEEE Photonics Technology Letters **20**, 1739–1741 (2008).
8. C. Qiu, J. Shu, Z. Li, X. Zhang, and Q. Xu, "Wavelength tracking with thermally controlled silicon resonators," Opt. Express **19**, 5143–5148 (2011).
9. J. A. Cox, A. L. Lentine, D. C. Trotter, and A. L. Starbuck, "Control of integrated micro-resonator wavelength via balanced homodyne locking," Opt. Express **22**, 11279–11289 (2014).
10. F. Morichetti, S. Grillanda, and A. Meloni, "Breakthroughs in photonics 2013: Toward feedback-controlled integrated photonics," IEEE Photonics Journal **2**, 1–6 (2014).
11. K. Padmaraju, D. F. Logan, and T. Shiraishi, J. J. Ackert, A. P. Knights, and K. Bergman, "Wavelength locking and thermally stabilizing microring resonators using dithering signals," Journal of Lightwave Technology **32**, 505–512 (2014).
12. S. Grillanda, M. Carminati, F. Morichetti, P. Ciccarella, A. Annoni, G. Ferrari, M. Strain, M. Sorel, M. Sampietro, and A. Melloni, "Non-invasive monitoring and control in silicon photonics using CMOS integrated electronics," Optica **1**, 129–136 (2014).
13. J. Fisher, A. Kodanev, and M. Nazarathy, "Multi-Degree-of-Freedom Stabilization of Large-Scale Photonic-Integrated Circuits," Journal of Lightwave Technology **33**, 2146–2166 (2015).
14. A. Mahendra, C. Xiong, X. Zhang, B. J. Eggleton, and P. H. W. Leong, "Dynamic thermal control of silicon nitride photonic integrated circuits," Australian Conference on Optical Fibre Technology (2015).
15. J. A. Juarez-Abad, J. Linares-Flores, E. Guzman-Ramirez, and H. Sira-Ramirez, "Generalized proportional integral tracking controller for a single-phase multilevel cascade inverter: An FPGA implementation," IEEE Transactions on Industrial Informatics **10**, 256–266 (2014).
16. K. A. Astrom, and B. Wittenmark, "Computer-controlled systems: theory and design," IEEE Transactions on Industrial Informatics, (2013).
17. http://au.mathworks.com/products/sysid/, "System Identification Toolbox," MathWorks, (2012).
18. J. C. Doyle, B. A. Francis, and A. R. Tannenbaum, "Generalized proportional integral tracking controller for a single-phase multilevel cascade inverter: An FPGA implementation," Courier Corporation, (2013).
19. L. Zhuang, D. Marpaung, M. Burla, W. Beeker, A. Leinse, and C. Roelofzen, "Low-loss, high-index-contrast Si 3 N 4/SiO 2 optical waveguides for optical delay lines in microwave photonics signal processing," Opt. Express **19**, 23162–23170 (2011).
20. J. C. Doyle, B. A. Francis, and A. R. Tannenbaum, "Feedback control theory," Courier Corporation, (2013).
21. S. Skogestad, and I. Postlethwaite, "Multivariable feedback control: analysis and design," Wiley New York **2**, (2007).
22. https://au.mathworks.com/help/control/ug/mimo-transfer-function-models.html, "MIMO Transfer Functions," MathWorks, (2016).
23. https://au.mathworks.com/help/control/functionlist.html, "Control System Toolbox Functions," MathWorks, (2016).
24. http://au.mathworks.com/videos/control-system-tuning-in-simulink-made-easy-81839.html, "Control system tuning in simulink made easy," MathWorks, (2014).
25. K. J. Astrom, and R. M. Murray, "Feedback systems: an introduction for scientists and engineers," Princeton university press, (2010).